Electronic Supplementary Material (ESI) for Environmental Science: Processes & Impacts.
This journal is © The Royal Society of Chemistry 2022

Supplementary Information

Extracellular Polymeric Substances Enhance Dissolution and Microbial Methylation of Mercury Sulfide Minerals

Zhanhua Zhang[1], Zhenyu Zhao[1], Qingxuan Fang[1], Ruohong Qiao[1], Tong Zhang[1]*

[1] College of Environmental Science and Engineering, Ministry of Education Key Laboratory of Pollution Processes and Environmental Criteria, Tianjin Key Laboratory of Environmental Remediation and Pollution Control, Nankai University, Tianjin 300350, P. R. China

* Corresponding author: Tel (Fax): +86 22-66229516; E-mail: zhangtong@nankai.edu.cn

Materials and Methods

Culturing of mercury methylating bacteria

Two mercury methylating bacteria, *Pseudodesulfovibrio mercurii* ND132 (Cynthia C. Gilmour, Smithsonian Environmental Research Center) and *Geobacter sulfurreducens* PCA (ATCC 51573), were utilized as the model microorganisms. *P. mercurii* ND132 cells were cultured in a sulfate reduction medium that contained 27 mmol L^{-1} pyruvate as electron donors and 20 mmol L^{-1} sulfate as electron acceptors, according to Gilmour *et al.* (2011).[1] *G. sulfurreducens* PCA cells were grown in a nutrient medium that contained 20 mmol L^{-1} acetate as electron donors and 40 mmol L^{-1} fumarate as electron acceptors, described by Lovley and Phillips (1988).[2] Both media were buffered with 19 mmol L^{-1} sodium 3-(N-morpholino)propanesulfonic acid (MOPS) at pH 7.2–7.4 during incubations. The anaerobic bottles sealed with Teflon-coated butyl rubber stopper and aluminum crimp caps were kept in dark, at room temperature (23–26 ℃) in a glove box (Coy Laboratory Products, U.S.A.). A microplate reader (Spark 10M, Tecan, Switzerland) was used to monitor bacterial growth.

Synthesis and characterization of cinnabar samples

Two different cinnabars (α-HgS) were utilized as the test minerals. Nano-cinnabar was synthesized using a sonochemical method according to Wang and Zhu (2004).[3] Briefly, 3.2 g $Hg(CH_3COO)_2{\cdot}2H_2O$, 3.6 g $Na_2S_2O_3$ and 5 mL triethanolamine were mixed in 95 mL nanopure water (18.2 MΩ·cm). Then, the mixture was sonicated for 60 min without any cooling. N_2 was bubbled through the reaction solution to purge the dissolved O_2. The precipitates were centrifuged, then thoroughly washed with absolute ethanol, acetone, and nanopure water. Bulk-cinnabar was purchased from Aladdin Bio-Chem Technology Co., Ltd., China, and washed with

5% (v/v) HNO_3, then thoroughly rinsed with nanopure water. The two cinnabars were freeze-dried, then sealed in the centrifuge tube, and stored in the glove box.

The crystallographic structures of the cinnabar samples were analyzed by X-ray diffraction (XRD, Ultima IV, Rigaku, Japan) on a diffractometer with Cu Kα radiation (λ = 1.5418 Å). Scanning electron microscopy (SEM, JSM-7800F, JEOL, Japan) and transmission electron microscopy (TEM, Tecnai G2 F20, FEI, U.S.A.) were utilized to characterize the morphology of two HgS minerals. The chemical compositions of two HgS were analyzed by energy-dispersive X-ray spectroscopy (EDX, JSM-7800F, JEOL, Japan) elemental mapping. X-ray photoelectron spectroscopy (XPS, ESCALAB 250Xi, Thermo Fisher, U.S.A.) was applied to analyze photoelectron binding energies, and spectra fitting was conducted using software package, Avantage v5.976. The surface areas of nano-cinnabar and bulk-cinnabar were determined using a surface area and porosity analyzer (ASAP 2460, Micromeritics, U.S.A.).

Table S1. Physicochemical properties of nano-cinnabar and bulk-cinnabar.

	Crystal facet	Crystallite size (nm) [a]	BET surface area (m^2 g^{-1}) [b]
Nano-cinnabar [c]	(011)	6.85 ± 0.24	14.76 ± 0.06 *
	(102)	8.13 ± 0.17	
Bulk-cinnabar [c]	(011)	45.73 ± 0.26 *	0.5 ± 0.06
	(102)	57.05 ± 0.26 *	

[a] Crystallite sizes were estimated from the broadening of XRD peaks by the Scherrer formula.

[b] BET surface areas were measured by N_2 adsorption using the Brunauer-Emmett-Teller (BET) method.

[c] Data represent mean ± 1 standard deviation (n = 3–4). Values that are statistically different ($p < 0.01$) between nano-cinnabar and bulk-cinnabar according to the two-sample *t*-test are indicated by asterisks.

Table S2. Characterization of extracellular polymeric substances (EPS) derived from *P. mercurii* ND132 and *G. sulfurreducens* PCA.

EPS properties	EPS(ND132) [a]	EPS(PCA) [a]
Protein/TOC (%)	54.76 ± 1.67 *	21.88 ± 1.46
Polysaccharide/TOC (%)	6.38 ± 0.42	17.37 ± 0.60 *
TN/TC (%)	5.46 ± 0.63 *	2.04 ± 0.21
TS/TC (%)	0.87 ± 0.04 *	0.32 ± 0.03
$SUVA_{280}$ (L (mg-C)$^{-1}$ m^{-1})	3.14 ± 0.02 *	1.69 ± 0.01
$S_{275–295}/S_{350–400}$	2.93 ± 0.52	4.04 ± 0.35 *

[a] Data represent mean ± 1 standard deviation (n = 3–4). Values that are statistically different ($p < 0.01$) between EPS(ND132) and EPS(PCA) according to the two-sample *t*-test are indicated by asterisks.

Table S3. XPS spectral features of C 1s and Hg 4f signals for nano-cinnabar in the absence and presence of EPS(ND132) or EPS(PCA).

	Signal	Assigned peak	Binding energy (eV)
EPS(ND132)	C 1s	C–C, C=C	284.8
		C–O, C–O–C	286.8
		O=C–O	288.8
	Hg 4f	Hg $4f_{5/2}$	104.8
		Hg $4f_{7/2}$	100.8
EPS(PCA)	C 1s	C–C, C=C	284.8
		C–O, C–O–C	286.7
		O=C–O	288.7
	Hg 4f	Hg $4f_{5/2}$	105.0
		Hg $4f_{7/2}$	101.0
No EPS addition	Hg 4f	Hg $4f_{5/2}$	105.2
		Hg $4f_{7/2}$	101.2

Table S4. Raman band positions and assignments for tryptophan and phenylalanine according to the references.

Amino acid	Band position	Band assignment	Reference
Tryptophan	1546–1561 cm^{-1}	C–C stretching vibration of pyrrole ring	Harz *et al.*, 2006; Xue *et al.*, 2008; Zhu *et al.*, 2011
	1418–1442 cm^{-1}	Stretching vibration of benzene/pyrrole ring	Okada *et al.*, 2001; Xue *et al.*, 2008; Chuang and Chen, 2009
	1355–1376 cm^{-1}	Fermi resonance between N–C stretching in pyrrole ring and combination bands of out-of-plane bending	Sato *et al.*, 2007; Harz *et al.*, 2008; Xue *et al.*, 2008
	1007–1015 cm^{-1}	Out-of-plane breathing vibration of benzene/pyrrole ring	Harz *et al.*, 2008; Sanchez *et al.*, 2008; Schlamadinger *et al.*, 2009
	755–764 cm^{-1}	In-plane breathing vibration of benzene/pyrrole ring	Harz *et al.*, 2006; Harz *et al.*, 2008; Schlamadinger *et al.*, 2011
Phenylalanine	1604–1608 cm^{-1}	In-plane stretching vibration of benzene ring	Harz *et al.*, 2006; Zhu *et al.*, 2011; Hernández *et al.*, 2013
	1207–1210 cm^{-1}	Side chain C–C stretching vibration	Harz *et al.*, 2006; Harz *et al.*, 2008; Hernández *et al.*, 2013
	1004–1007 cm^{-1}	Out-of-plane breathing vibration of benzene ring	Harz *et al.*, 2006; Harz *et al.*, 2008; Hernández *et al.*, 2013

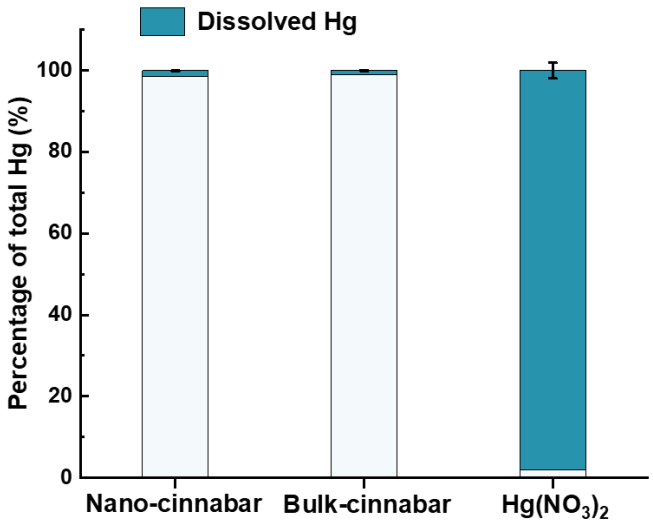

Fig. S1. Fraction of the total mercury after the samples were centrifugated at 14000 rpm for 30 min. The nano-cinnabar and bulk-cinnabar samples consisted of 0.5 g L^{-1} cinnabar without the addition of EPS. The $Hg(NO_3)_2$ sample consisted of 8 μg L^{-1} $Hg(NO_3)_2$ and 15 mg-C L^{-1} EPS.

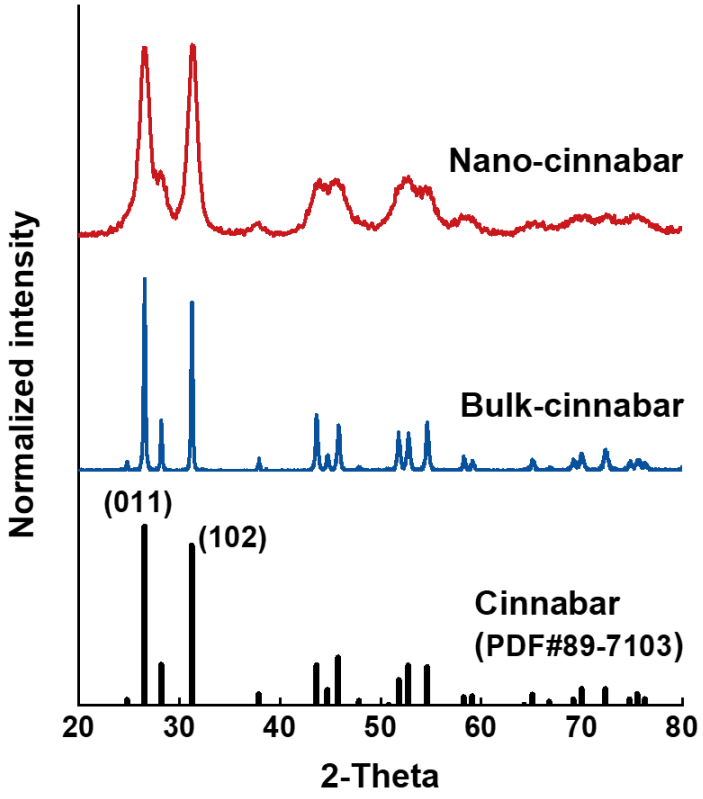

Fig. S2. XRD spectra of nano-cinnabar and bulk-cinnabar.

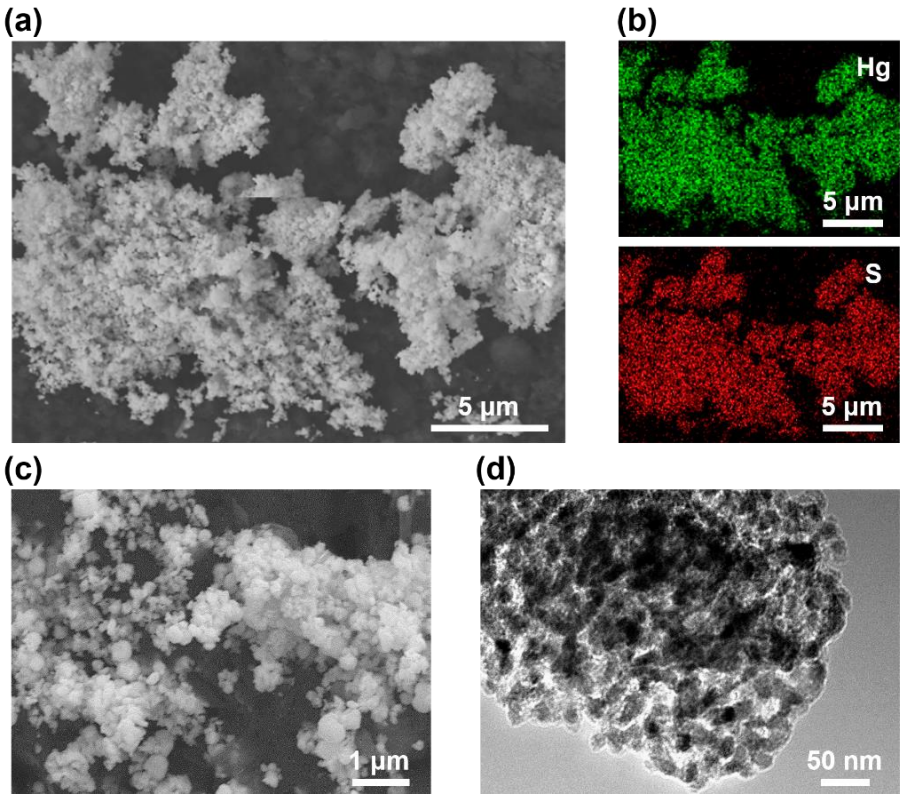

Fig. S3. SEM images (a, c), EDX elemental mapping (b), and TEM image (d) of nano-cinnabar.

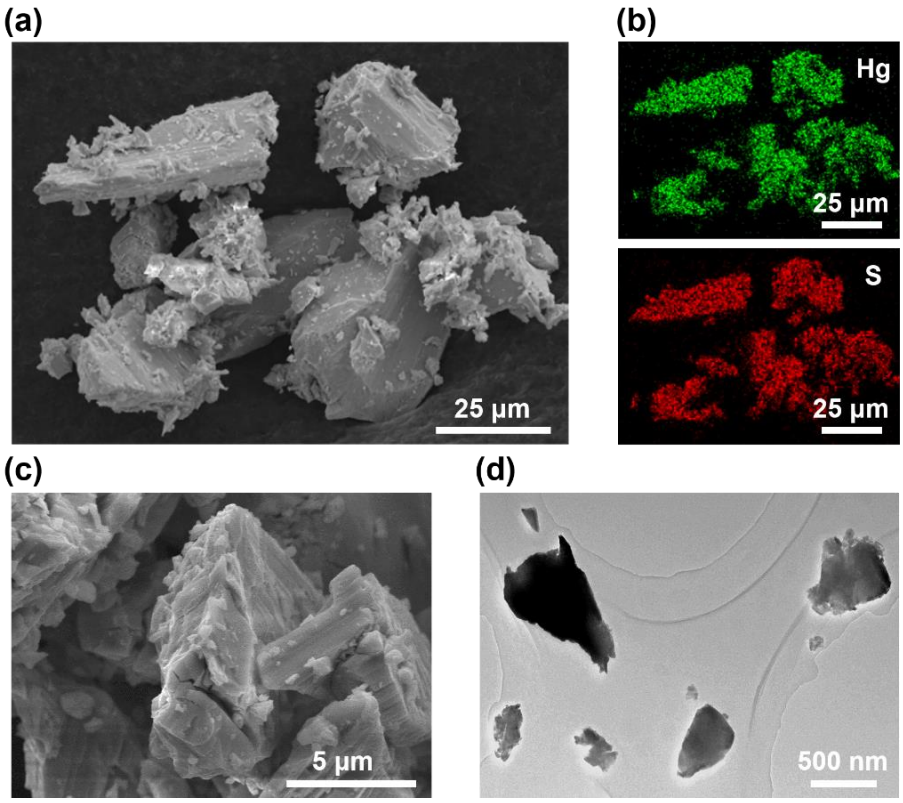

Fig. S4. SEM images (a, c), EDX elemental mapping (b), and TEM image (d) of bulk-cinnabar.

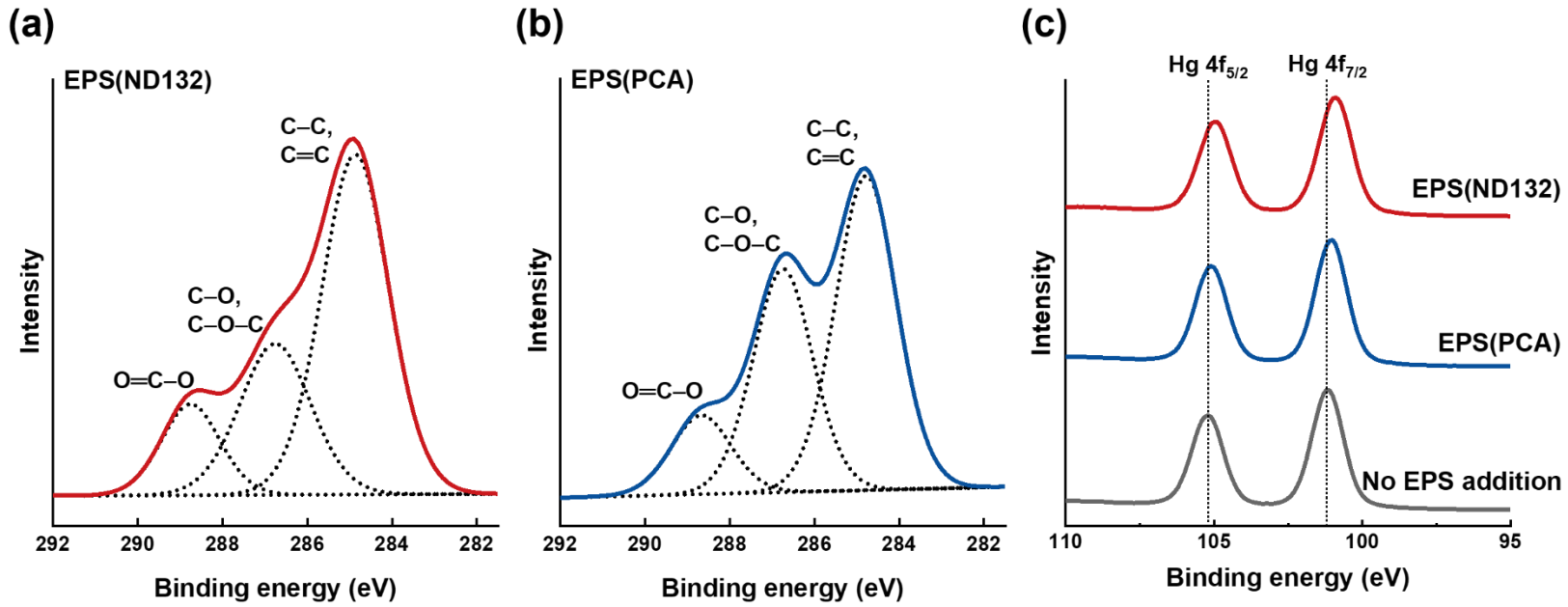

Fig. S5. XPS spectra of C 1s signals of nano-cinnabar in the presence of EPS(ND132) (a) or EPS(PCA) (b). XPS spectra of Hg 4f signals (c) of nano-cinnabar in the absence and presence of EPS(ND132) or EPS(PCA).

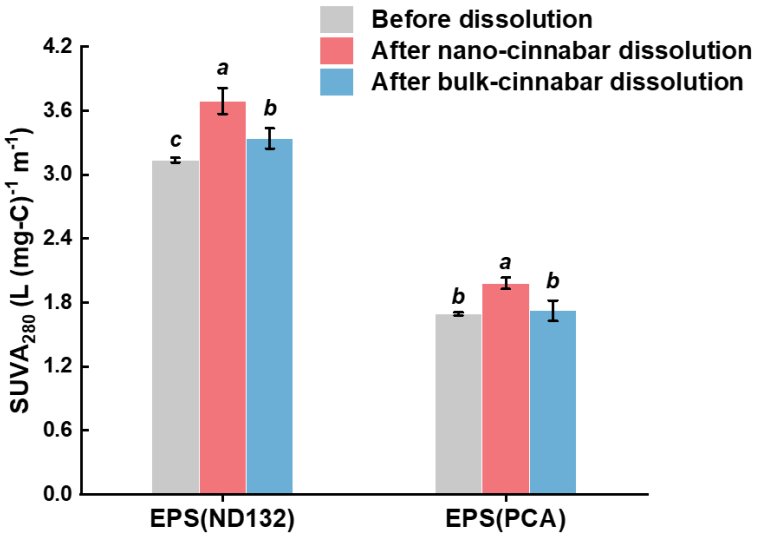

Fig. S6. $SUVA_{280}$ values of EPS(ND132) and EPS(PCA) solutions before and after the dissolution of nano-cinnabar and bulk-cinnabar. Error bars represent ± 1 standard deviation of replicate samples (n = 3–4). Values that are statistically different ($p < 0.01$) according to the one-way analysis of variance (ANOVA) are indicated by italic lowercase letters.

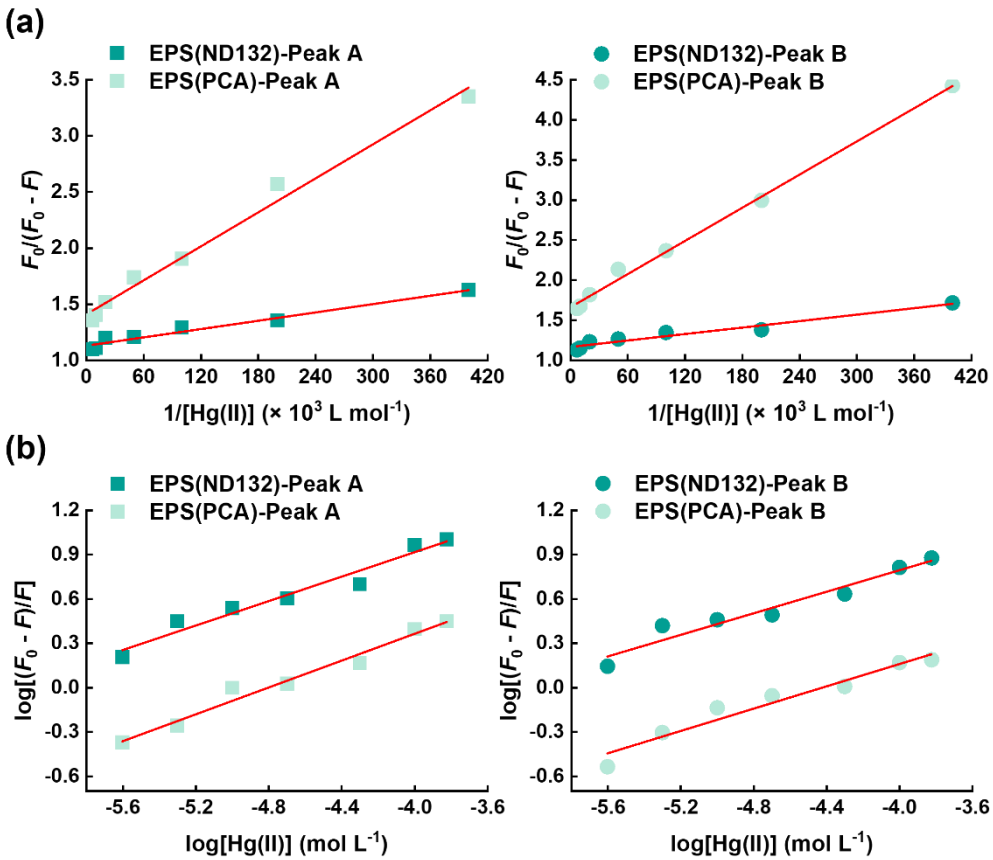

Fig. S7. The modified Stern-Volmer plots (a) and static quenching data fitting (b) for fluorescence quenching of peak A and peak B in EEM fluorescence spectra of EPS(ND132) and EPS(PCA). The red solid lines represent the linear regression fitting of fluorescence data.

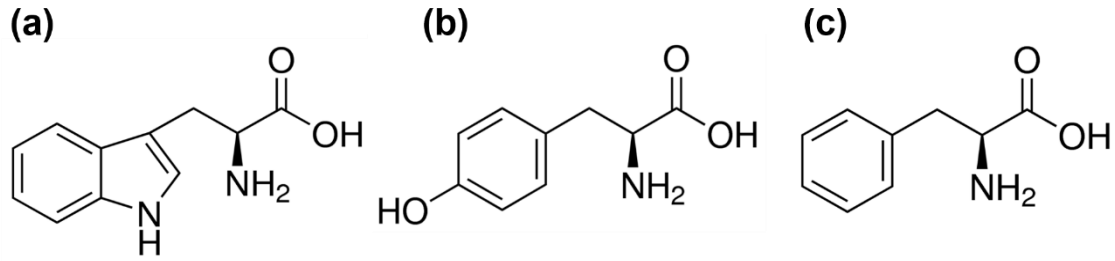

Fig. S8. Structural formula of aromatic amino acids. (a) Tryptophan, (b) Tyrosine, and (c) Phenylalanine.

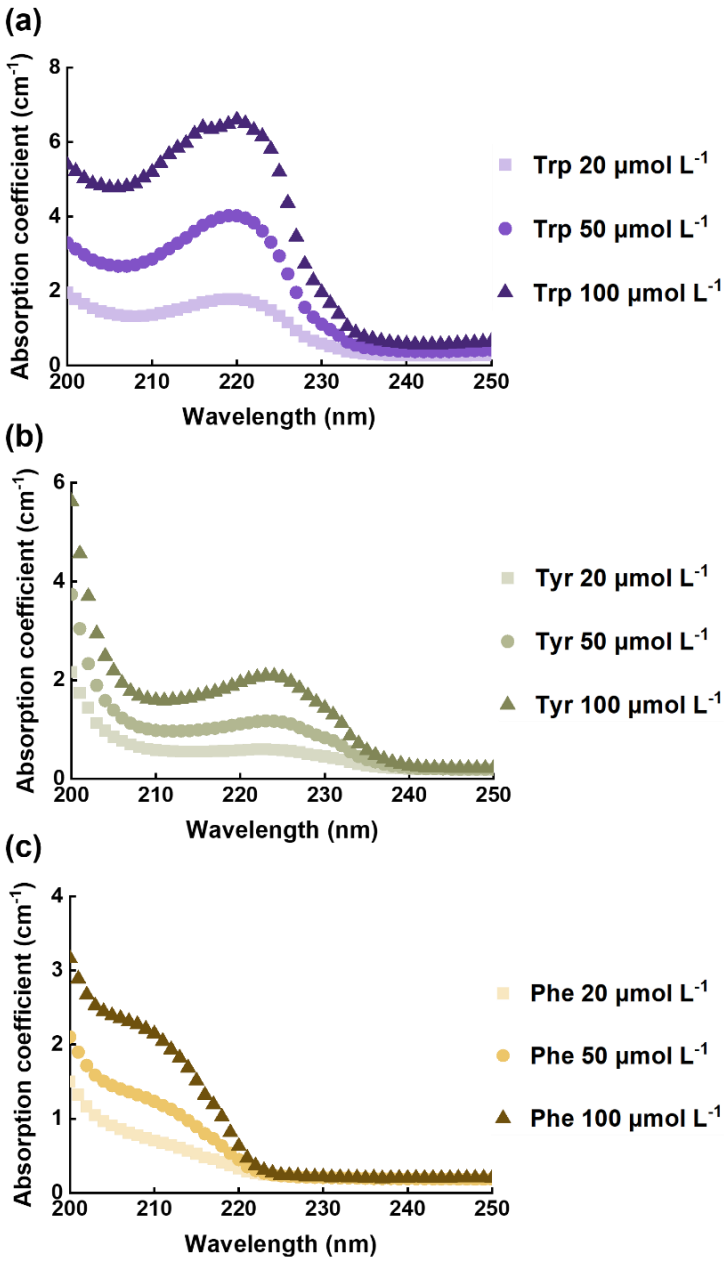

Fig. S9. Ultraviolet absorption spectra of tryptophan (a), tyrosine (b), and phenylalanine (c) at different concentrations of aromatic amino acid. The absorption coefficient (a, cm^{-1}) is converted from the absorbance (A) followed by the equation $a = 2.303A/l$, where l is the path length (cm).

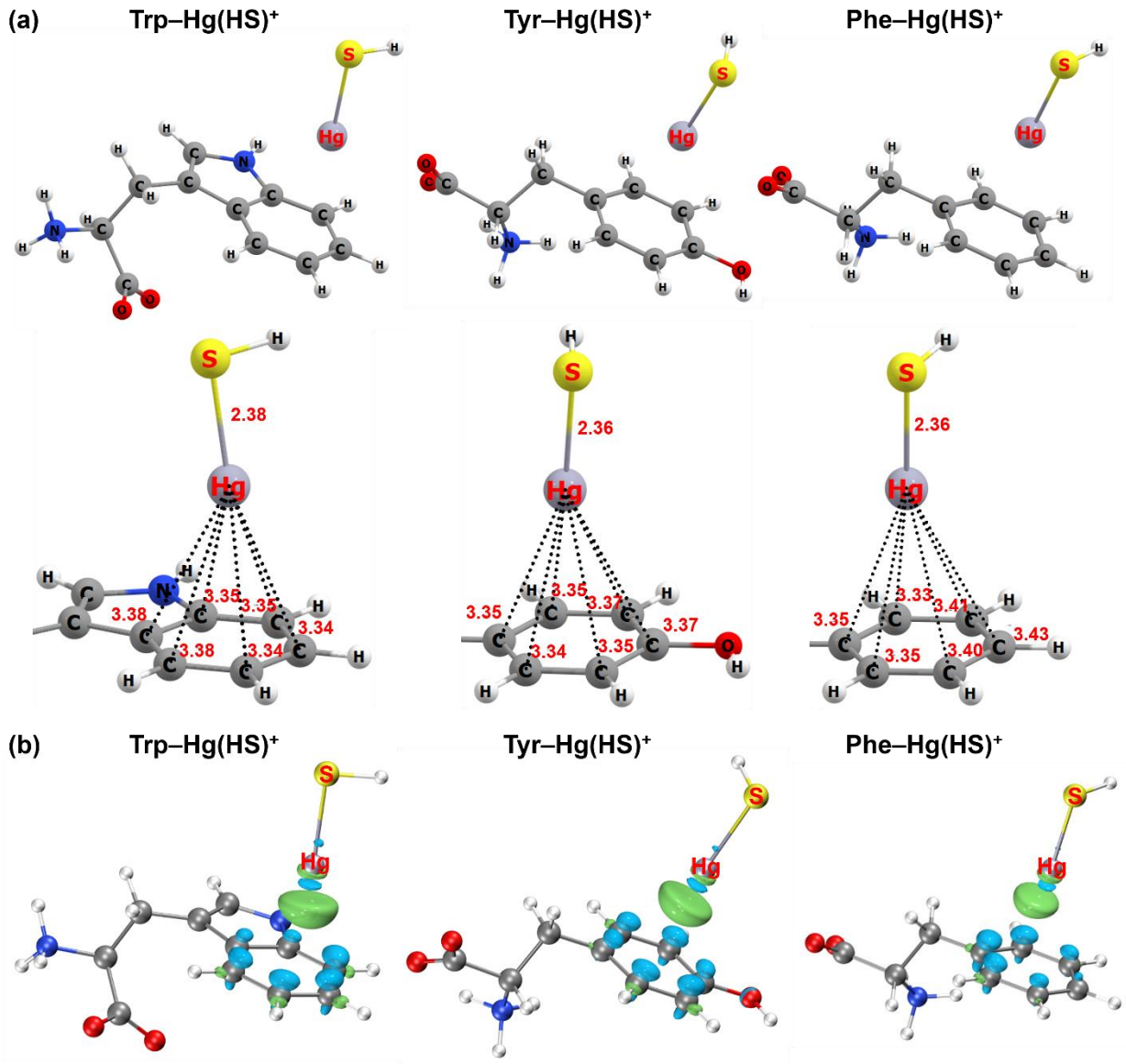

Fig. S10. The optimized ground-state geometry structures (a) and electron density difference maps (b) of the cation-π complexes formed between aromatic structures of three amino acids and $Hg(HS)^+$. The unit of distance between Hg atom and C atom in (a) is Å. The light green and light blue colors in (b) represent electron accumulation and electron depletion, respectively. The isosurface value (ρ) of electron density difference is 0.001 au.

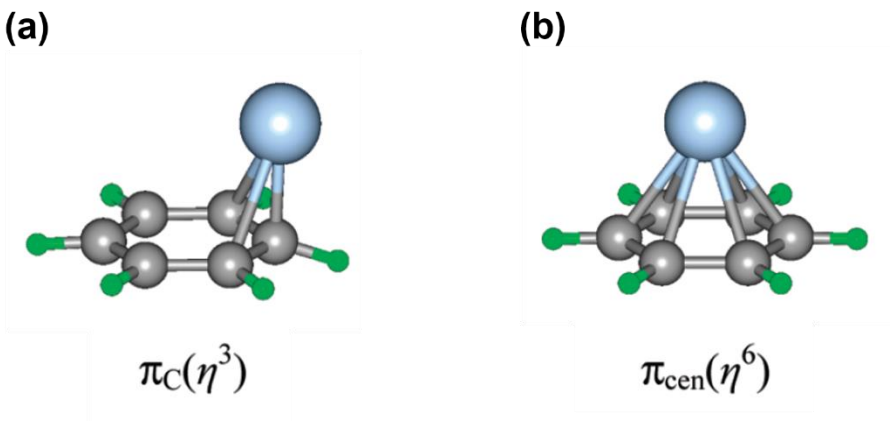

Fig. S11. The $\pi_C(\eta^3)$ (a) and $\pi_{cen}(\eta^6)$ geometry structures of the cation-π complexes formed between benzene and transition metal cation (adapted from Yi *et al.*, 2009). The light blue and gray spheres represent transition metal cation and carbon atom, respectively.

References

1. C. C. Gilmour, D. A. Elias, A. M. Kucken, S. D. Brown, A. V. Palumbo, C. W. Schadt and J. D. Wall, Sulfate-reducing bacterium *Desulfovibrio desulfuricans* ND132 as a model for understanding bacterial mercury methylation, *Appl. Environ. Microbiol.*, 2011, **77**, 3938-3951.
2. D. R. Lovley and E. J. P. Phillips, Novel mode of microbial energy metabolism: Organic carbon oxidation coupled to dissimilatory reduction of iron or manganese, *Appl. Environ. Microbiol.*, 1988, **54**, 1472-1480.
3. H. Wang and J. Zhu, A sonochemical method for the selective synthesis of alpha-HgS and beta-HgS nanoparticles, *Ultrason. Sonochem.*, 2004, **11**, 293-300.
4. C. Chuang and Y. Chen, Raman scattering of L-tryptophan enhanced by surface plasmon of silver nanoparticles: Vibrational assignment and structural determination, *J. Raman Spectrosc.*, 2009, **40**, 150-156.
5. M. Harz, R. A. Claus, C. L. Bockmeyer, M. Baum, P. Rösch, K. Kentouche, H. P. Deigner and J. Popp, UV-resonance Raman spectroscopic study of human plasma of healthy donors and patients with thrombotic microangiopathy, *Biopolymers*, 2006, **82**, 317-324.
6. M. Harz, M. Krause, T. Bartels, K. Cramer, P. Rösch and J. Popp, Minimal invasive gender determination of birds by means of UV-resonance Raman spectroscopy, *Anal. Chem.*, 2008, **80**, 1080-1086.
7. B. Hernández, F. Pflüger, S. G. Kruglik and M. Ghomi, Characteristic Raman lines of phenylalanine analyzed by a multiconformational approach, *J. Raman Spectrosc.*, 2013, **44**, 827-833.
8. A. Okada, T. Miura and H. Takeuchi, Protonation of histidine and histidine-tryptophan

interaction in the activation of the M2 ion channel from influenza a virus, *Biochemistry*, 2001, **40**, 6053-6060.

9. K. M. Sanchez, T. J. Neary and J. E. Kim, Ultraviolet resonance Raman spectroscopy of folded and unfolded states of an integral membrane protein, *J. Phys. Chem. B*, 2008, **112**, 9507-9511.

10. A. Sato, Y. Gao, T. Kitagawa and Y. Mizutani, Primary protein response after ligand photodissociation in carbonmonoxy myoglobin, *Proc. Natl. Acad. Sci. U.S.A.*, 2007, **104**, 9627-9632.

11. D. E. Schlamadinger, M. M. Daschbach, G. W. Gokel and J. E. Kim, UV resonance Raman study of cation-π interactions in an indole crown ether, *J. Raman Spectrosc.*, 2011, **42**, 633-638.

12. D. E. Schlamadinger, J. E. Gable and J. E. Kim, Hydrogen bonding and solvent polarity markers in the UV resonance Raman spectrum of tryptophan: Application to membrane proteins, *J. Phys. Chem. B*, 2009, **113**, 14769-14778.

13. Y. Xue, A. V. Davis, G. Balakrishnan, J. P. Stasser, B. M. Staehlin, P. Focia, T. G. Spiro, J. E. Penner-Hahn and T. V. O'Halloran, Cu(I) recognition via cation-pi and methionine interactions in Cusf, *Nat. Chem. Biol.*, 2008, **4**, 107-109.

14. G. Zhu, X. Zhu, Q. Fan and X. Wan, Raman spectra of amino acids and their aqueous solutions, *Spectrochim. Acta, Part A*, 2011, **78**, 1187-1195.

15. H. Yi, H. M. Lee, and K. S. Kim, Interaction of benzene with transition metal cations: Theoretical study of structures, energies, and IR spectra, *J. Chem. Theory Comput.*, 2009, **5**, 1709-1717.